Supporting Information

Design of light-sensitive tubular MoS_2/C composite as the cathode for photo-enhanced rechargeable zinc-ion battery

*Mengjue Cao, Duoyin Wang, Yi Feng, Xiaoli Gu and Jianfeng Yao**

Jiangsu Co-Innovation Center of Efficient Processing and Utilization of Forest Resources, College of Chemical Engineering, Nanjing Forestry University, Nanjing 210037, China

*Corresponding author. Email: jfyao@njfu.edu.cn

1. Supplemental Experimental Procedures

1.1 Photo-responsive solid-state zinc-ion device

In this device, the gel electrolyte was prepared by dissolving 1.0 g polyvinyl alcohol (PVA, Mw: ~89000-98000) in 20 mL $ZnSO_4$ aqueous solution (2 M) under vigorous stirring at 90 °C for 2 h. The cathode was fabricated by coating MoS_2/C-NT slurry on the PET/ITO substrate and Zn foil act as anodes (mass loading: 2 mg cm^{-2}). The photo-responsive solid-state zinc-ion battery (PRZB) was assembled by sandwiching a gel electrolyte film of $ZnSO_4$- (PVA) between metal Zn and MoS_2/C-NT electrodes. The device was further sealed with 3M tape to prevent any gel electrolyte leakage. Cu conductive adhesive tape was tightly pasted to the margins of these electrodes.

1.2 Calculation of capacitive contribution in total capacitance

The contribution of the capacitive-controlled reaction can be estimated according to the following equations proposed by Dunn.

$$i(v) = k_1 v + k_2 v^{1/2} \quad (1)$$

where i is the current (A g^{-1}), v is the scan rate (mV s^{-1}), and k_1v and $k_2v^{1/2}$ correspond to the capacitive and diffusion contributions, respectively. The surface-controlled capacitance also reflects the rate performance of the electrode materials as well as the surface charge storage capability.

1.3 Calculation of conduction band

Generally, the hydrogen reduction potential is at 4.5 eV below the vacuum level. Therefore, the MoS_2 edge positions related to the vacuum level can be expressed empirically by the following equation:[1]

$$E_{CB} = E_{VB} + E_g \quad (2)$$

The calculated edge positions of VB_{MoS_2} and CB_{MoS_2} were -3.59 eV (vs. vacuum) and -1.69 eV (vs. vacuum), respectively.

1.4 Calculation of photo-conversion efficiency

To demonstrate the contribution of photo-regulation in the photo-electrochemical coupling process, photo-conversion efficiency has been calculated by the following equation:[2]

$$\eta = \frac{E_S S_1}{P_{in} t s_2} \times 100\% \quad (3)$$

where η represents the photo-conversion efficiency, E_S is the areal energy density at a specific current of 0.1 mA cm^{-2}, S_1 is the photo positive electrode area, P_{in} is the photo-power density, t is the charging time under illuminated condition, and S_2 is the illuminated surface area. As a result, the photo-conversion efficiency was calculated to be 0.98 % according to the experimental parameters.

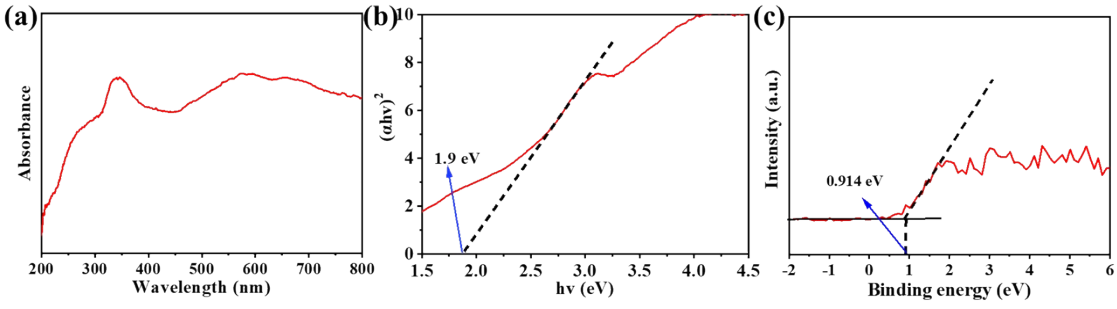

Fig. S1 UV−vis absorption spectrum (a) and Tauc plot of MoS_2 (b) and valence band XPS spectra (c).

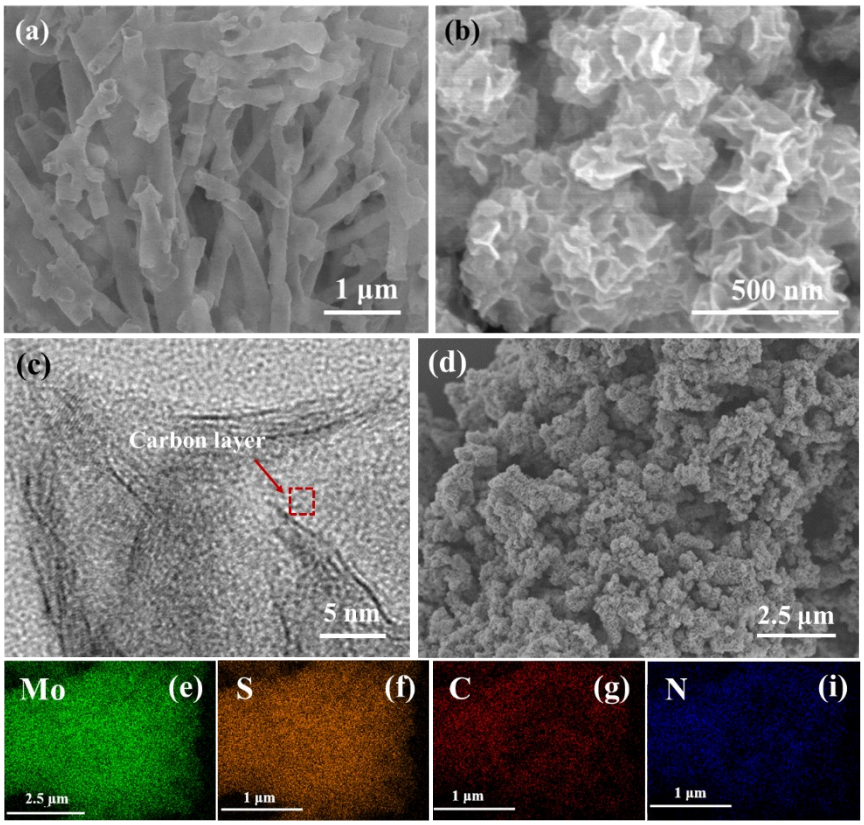

Fig. S2 SEM images of g-C_3N_4-NT (a) and MoS_2 (b), HRTEM image of MoS_2/C-NT (c), and SEM element mapping (d-i).

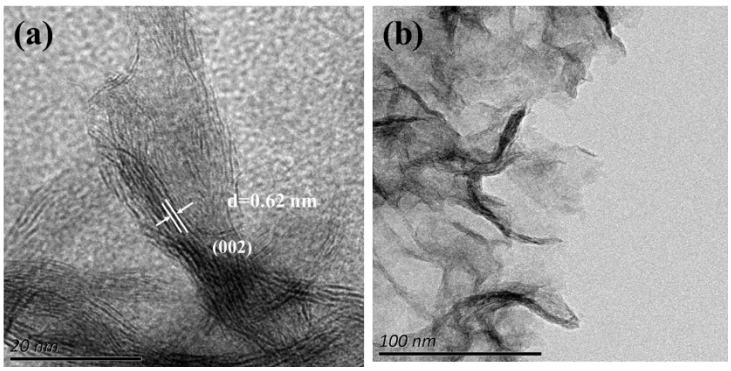

Fig. S3 HRTEM image of MoS_2/C-NT (a) and TEM image of MoS_2(b).

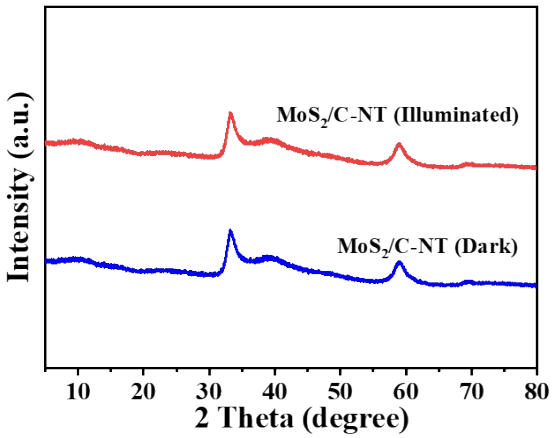

Fig. S4 XRD patterns of MoS_2/C-NT after light illumination.

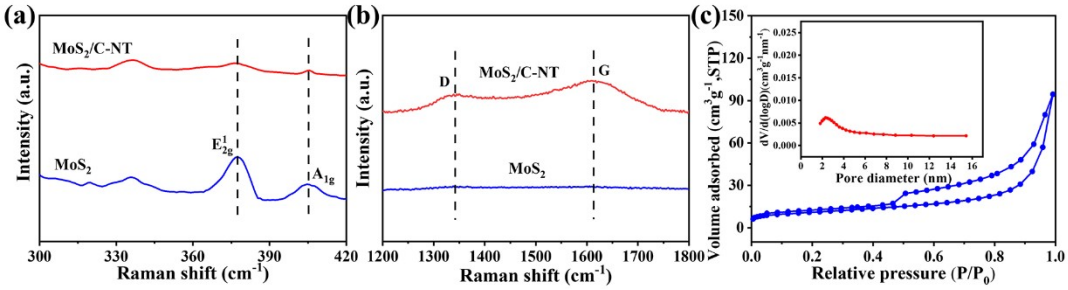

Fig. S5 Raman spectra of MoS_2 and MoS_2/C-NT with different range of Raman shift (300-420cm^{-1}) (a) and (1200-1800cm^{-1}) (b) and N_2 adsorption-desorption isotherm (inset: pore size distribution) (c).

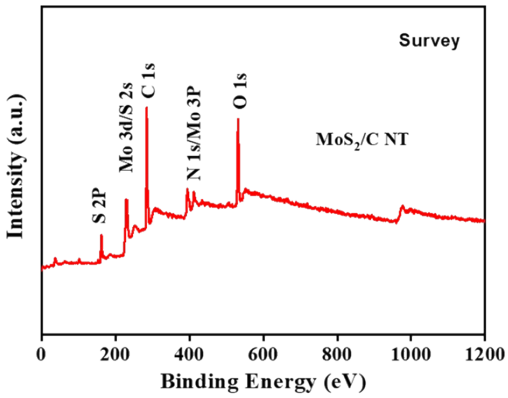

Fig. S6 XPS survey spectrum of MoS_2/C-NT.

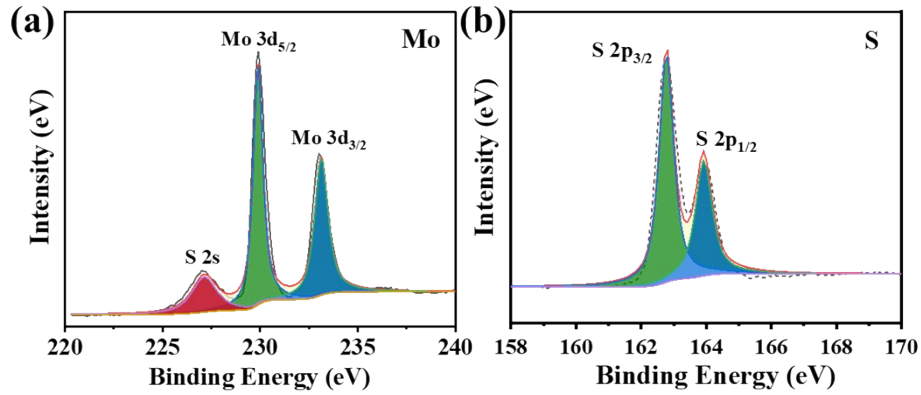

Fig. S7 High resolution XPS spectra of (a) Mo 3d and (b) S 2p of the MoS_2.

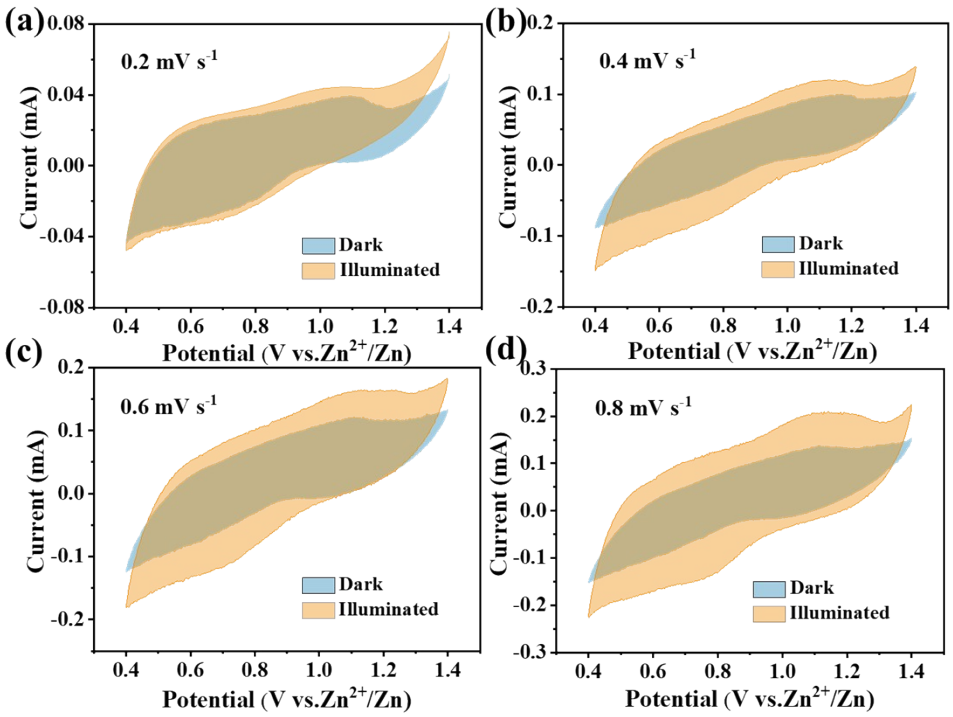

Fig. S8 CV curves of the photo-ZIBs at scan rates of 0.2 mV s^{-1} (a), 0.4 mV $^{-1}$ (b), 0.6 mV s^{-1} (c) and 0.8 mV s^{-1} (d) in dark and illuminated states.

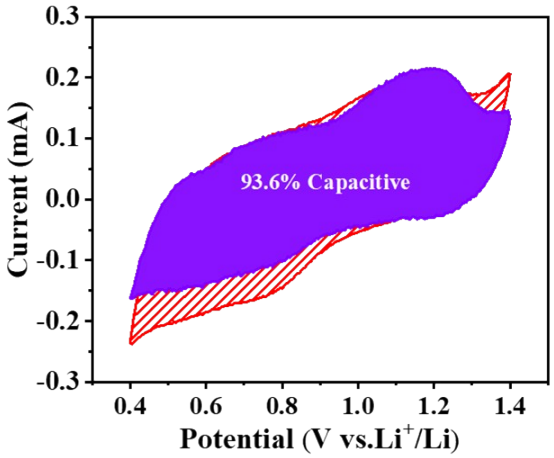

Fig. S9 Capacitive contribution determinations to charge storage at 0.8 mV s^{-1} under illuminated conditions.

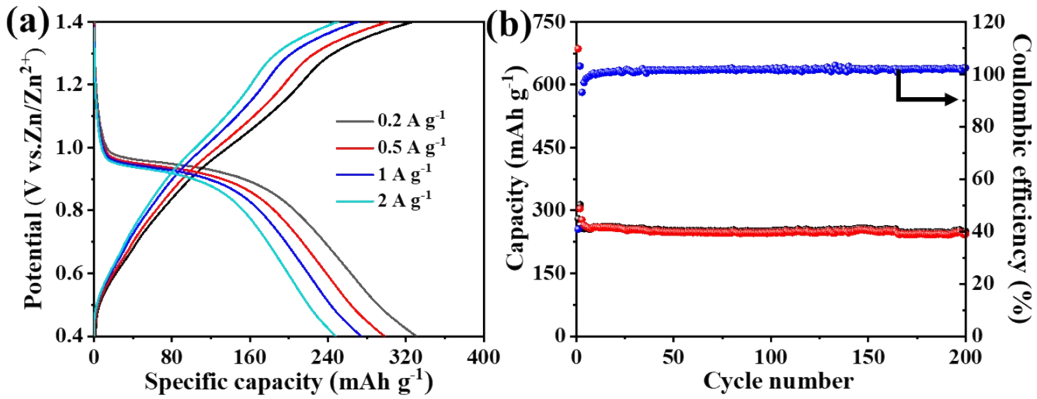

Fig. S10 Galvanostatic charge–discharge curves of MoS_2/C-NT at current densities of 0.2-2 A g^{-1} (a) and cycling performance of MoS_2/C-NT at 1A g^{-1} (b) under light condition.

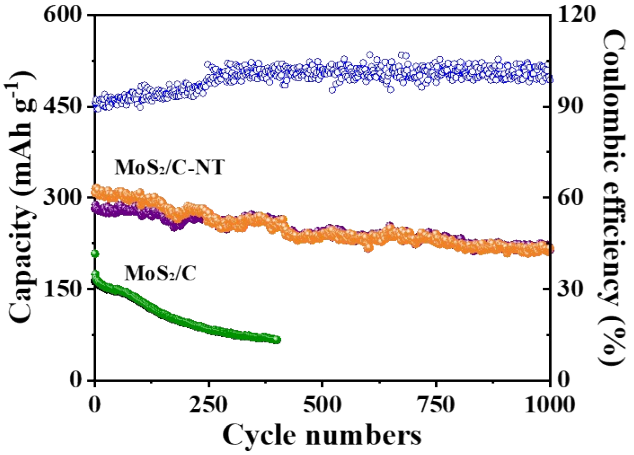

Fig. S11 Long-term cycling test of the MoS_2/C-NT and MoS_2/C at a specific current of 500 mA g^{-1} in dark.

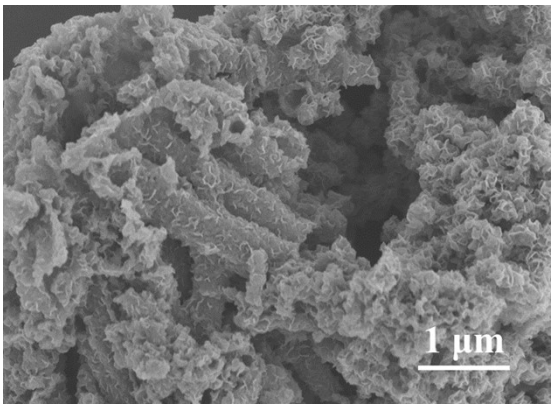

Fig. S12 SEM images of the cycled photocathode for 200 cycles under light condition.

GITT measurements:

During GITT test, the cell was discharged and charged at 0.1 A g^{-1} for 15min, and then relaxed for 30 min to allow the voltage to reach equilibrium. The Zn^{2+} diffusion coefficient (D_{Zn}^{2+}) can be calculated by the following equation:[3]

$$D=\frac{4}{\pi t}\left(\frac{m_B V_M}{M_B S}\right)^2\left(\frac{\Delta E_s}{\Delta E_\tau}\right)^2$$

Where V_M, M_B, m_B and S represent the molar volume of the active material, molar mass of the active material, mass of the active material and contact surface area of the anode, respectively; τ represents the relaxation time, and ΔEs and ΔEτ are the voltage difference during the pulse time and constant current charge/discharge process.

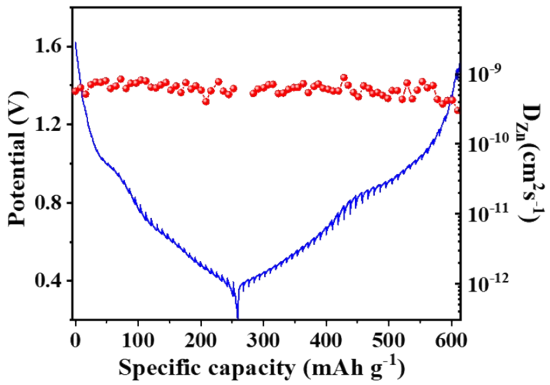

Fig. S13 Discharge/charge GITT profiles at 0.1 A g^{-1} and the corresponding Zn^{2+} diffusion coefficients of MoS_2/C-NT.

Table S1. A summary of the important parameters and performance of the recently reported photo-actuated batteries.

Positive electrode	Battery System	Current density (mA g^{-1})	Discharge capacity (mA h g^{-1})	Photo power density (Mw cm^{-2})	Cycling stability	Conversion efficiency (%)	Battery Type
N719 dye/$LiFePO_4$ [4]	Li	C/24		100	15	0.06-0.08	Coin cell
$(C_6H_9C_2H_4NH_3)_2$ PbI_4 [5]	Li	40	~90-100	100	10	0.034	pouch cell
TiO_2/dye/Cu_2S [6]	Li		150	100	10	~ 0.1	Coin cell
V_2O_5 [7]	Li	500	127	100		0.22	Coin cell
V_2O_5 [2]	Zn	50	370	12		1.2	Coin cell
VO_2 [8]	Zn	5000	190	12	250	0.18	Coin cell
NT-COF[9]	Li		100	100	100		Coin cell
Li_xTiO_2 nanoparticle [10]	Li	47	240				Coin cell
C60@POC [11]	Li		184	200	100	~1.0	Coin cell
MnO_2 [12]	Al	100	531	100	10	1.2	Coin cell
This work	Zn	500	216	100	200	0.98	Coin cell

References

1. R. Z. Yaqin Wang, Jianbao Li, Liangliang Li, Shiwei Lin *Nanoscale Research Letters volume*, 2014, **9**, 1-8.
2. B. D. Boruah, A. Mathieson, B. Wen, S. Feldmann, W. M. Dose and M. De Volder, *Energy Environ. Sci.*, 2020, **13**, 2414-2421.
3. F. Li, H. Ma, H. Sheng, Z. Wang, Y. Qi, D. Wan, M. Shao, J. Yuan, W. Li, K. Wang, E. Xie and W. Lan, *Small*, 2023, 202306276.
4. A. Paolella, C. Faure, G. Bertoni, S. Marras, A. Guerfi, A. Darwiche, P. Hovington, B. Commarieu, Z. Wang, M. Prato, M. Colombo, S. Monaco, W. Zhu, Z. Feng, A. Vijh, C. George, G. P. Demopoulos, M. Armand and K. Zaghib, *Nat. Commun.*, 2017, **8**, 14643.
5. S. Ahmad, C. George, D. J. Beesley, J. J. Baumberg and M. De Volder, *Nano Lett.*, 2018, **18**, 1856-1862.
6. C. Xu, X. Zhang, L. Duan, X. Zhang, X. Li and W. Lu, *Nanoscale*, 2020, **12**, 530-537.
7. B. D. Boruah, B. Wen and M. De Volder, *Nano Lett.*, 2021, **21**, 3527-3532.
8. B. Deka Boruah, A. Mathieson, S. K. Park, X. Zhang, B. Wen, L. Tan, A. Boies

and M. De Volder, *Adv. Energy Mater.*, 2021, **11**,2100115.
9. J. Lv, Y. X. Tan, J. Xie, R. Yang, M. Yu, S. Sun, M. D. Li, D. Yuan and Y. Wang, *Angew. Chem. Int. Ed.*, 2018, **57**, 12716-12720.
10. C. Andriamiadamanana, I. Sagaidak, G. Bouteau, C. Davoisne, C. Laberty-Robert and F. Sauvage, *Advanced Sustainable Systems*, 2018, **2**, 1700166.
11. X. Zhang, K. Su, A. G. A. Mohamed, C. Liu, Q. Sun, D. Yuan, Y. Wang, W. Xue and Y. Wang, *Energ. Environ. Sci.*, 2022, **15**, 780-785.
12. X. Zhang, W.L. Song, M. Wang, J. Tu, H. Jiao and S. Jiao, *Energy Storage Mater.*, 2022, **45**, 586-594.